Current Biology 23, 1173–1180, July 8, 2013 ©2013 Elsevier Ltd All rights reserved http://dx.doi.org/10.1016/j.cub.2013.05.015

Article

Local Cytoskeletal and Organelle Interactions Impact Molecular-Motor-Driven Early Endosomal Trafficking

Allison L. Zajac,[1] Yale E. Goldman,[1] Erika L.F. Holzbaur,[1,*] and E. Michael Ostap[1,*]
[1]The Pennsylvania Muscle Institute and Department of Physiology, Perelman School of Medicine, University of Pennsylvania, Philadelphia, PA 19104-6085, USA

Summary

Background: In the intracellular environment, motor-driven cargo must navigate a dense cytoskeletal network among abundant organelles.
Results: We investigated the effects of the crowded intracellular environment on early endosomal trafficking. Live-cell imaging of an endosomal cargo (endocytosed epidermal growth factor-conjugated quantum dots) combined with high-resolution tracking was used to analyze the heterogeneous motion of individual endosomes. The motile population of endosomes moved toward the perinuclear region in directed bursts of microtubule-based, dynein-dependent transport interrupted by longer periods of diffusive motion. Actin network density did not affect motile endosomes during directed runs or diffusive interruptions. Simultaneous two-color imaging was used to correlate changes in endosomal movement with potential obstacles to directed runs. Termination of directed runs spatially correlated with microtubule-dense regions, encounters with other endosomes, and interactions with the endoplasmic reticulum. During a subset of run terminations, we also observed merging and splitting of endosomes, deformation of the endoplasmic reticulum, and directional reversals at speeds up to 10-fold greater than characteristic in vitro motor velocities. These observations suggest that endosomal membrane tension is high during directed run termination.
Conclusions: Our results indicate that the crowded cellular environment significantly impacts the motor-driven motility of organelles. Rather than simply acting as impediments to movement, interactions of trafficking cargos with intracellular obstacles may facilitate communication between membrane-bound compartments or contribute to the generation of membrane tension necessary for fusion and fission of endosomal membranes or remodeling of the endoplasmic reticulum.

Introduction

Molecular-motor-driven intracellular trafficking of cargos is essential for maintaining cellular homeostasis [1]. In vitro analyses of molecular motors have provided insight into intrinsic movement characteristics such as directionality, run length, speed, and force sensitivity [2]. However, motility in the cell is strongly affected by the organization and dynamics of cytoskeletal tracks [3–5], interactions with other organelles [6], and crowding in the cytoplasm [7]. Thus, characterization of the full range of motion of individual cargo is needed to understand how intracellular obstacles and organelle interactions impact directed transport.

To investigate the movement of single cargos in live cells, we focused on the trafficking of epidermal growth factor (EGF) in early endosomes. After EGF activates its receptor (EGFR), the two are endocytosed, transported through the endosomal system from early to late endosomes, and ultimately degraded in lysosomes [8]. Both actin- and microtubule (MT)-based motors are associated with early endosomes, including myosin Vb [9], myosin VI [10], myosin Ib [11], kinesin-1 [12], kinesin-2 [12], KIF16b [13], and dynein [12, 14, 15]. Early endosomes exhibit a complex mixture of dynein-driven directed runs toward the perinuclear region interrupted by intervals of little net transport [16]. The goal of the present study is to characterize the full spectrum of motions exhibited by individual early endosomes to provide insight into (1) why directed motion is interrupted, (2) what types of residual movement are occurring during the interruptions, and (3) what functional roles the combination of directed runs and interruptions play in endosomal trafficking and maturation.

We measured early endosomal trajectories using high temporal and spatial resolution imaging and developed objective methods to analyze distinct phases of motion within single trajectories. We found that a subpopulation of early endosomes exhibited mostly confined motion, regulated by the density of the actin network. In contrast, the motile population of early endosomes exhibited a combination of directed, dynein-dependent movement interspersed with longer diffusive pauses. We observed spatial overlap between sites of pausing and regions of dense MTs, other early endosomes, and the endoplasmic reticulum (ER), suggesting that these cellular factors may interrupt directed runs. Further, these interactions and the associated pauses in directed motion may play functional roles in endosomal maturation and sorting.

Results

Intracellular Dynamics of Early Endosomes

We surveyed the dynamics within the early endosomal population using high-speed (20 frames per second [fps]) imaging in Arpe-19 cells, a human epithelial cell line with an actin-rich cortex and a polarized MT array (Figure S1A available online). Several fluorescent markers (Rab5 and endocytosed EGF) were compared to ensure that our labeling strategy did not introduce artifactual movements or perturb the trafficking kinetics of endocytosed transferrin (Figure S1B). Early endosomes could be divided into two groups based on their movement. An immotile subpopulation covered little distance over the period of observation (<0.5 μm over 45 s). A motile subpopulation moved in short, perinuclear-directed bursts interrupted by periods of little net displacement, which we will refer to as pauses (Figure 1A and Movie S1). Analysis of 2,839 trajectories from GFP-Rab5-positive early endosomes in ten cells (Figure 1B) showed that 62% ± 2% (mean ± SEM) are immotile (Table S1). In the motile population, 78% ± 4% of rapid movements were directed toward the perinuclear region, where the majority of MT minus ends are located (Table S1). The dependence of this rapid transport on dynein/dynactin [16] was

*Correspondence: holzbaur@mail.med.upenn.edu (E.L.F.H.), ostap@mail.med.upenn.edu (E.M.O.)

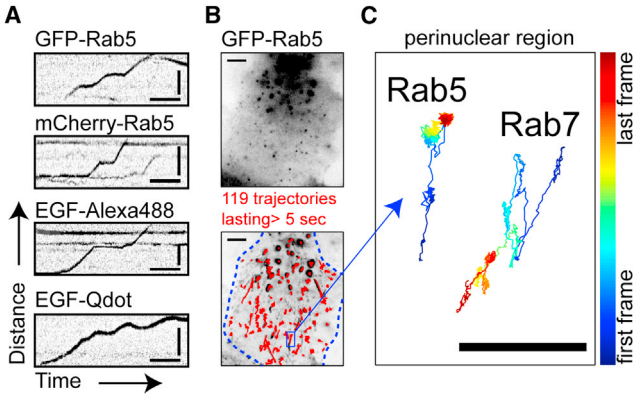

Figure 1. Motility in the Early Endosomal Population

(A) Early endosomes move in rapid bursts toward the perinuclear region interrupted by periods of little net movement. Kymographs of early endosomes were contrast inverted and background subtracted. See also Movie S1. Scale bars represent 2 s and 5 μm.

(B) Tracking of GFP-Rab5 movements for analysis. GFP-Rab5-positive early endosomes (single frame in top panel). Bottom panel: maximum-intensity projection of GFP-Rab5 movie (45 s) overlaid with trajectories (red) and cell outline (blue). Scale bars represent 5 μm.

(C) Early endosomes exhibit rapid movements toward the perinuclear region, while late endosomes/lysosomes exhibit bidirectional rapid movements. Representative Rab5 and Rab7 trajectories from the cell in (B) are shown, color coded for time (blue, first frame; red, last frame). The cellular location of the Rab5 trajectory is indicated in (B) with a blue box. The scale bar represents 2 μm. See also Figures S1E and S1F and Table S1.

See also Figure S1, Table S1, and Movie S1.

confirmed by expression of the dominant-negative construct CC1 (the coiled-coiled-1 domain of $p150^{Glued}$) to disrupt dynein/dynactin function (Movie S1), although other motors such as myosin VI and KIF16b are also present (Figures S1C and S1D). For comparison, late endosomes/lysosomes labeled with several markers, including the GTPase Rab7, underwent significantly more bidirectional movement than early endosomes (Figures 1C, S1E, and S1F and Table S1).

To allow tracking at higher resolution, we labeled early endosomes with endocytosed EGF-conjugated quantum dots (EGF-Qdots; Figure 1A). Interpretation of complex motion inside cells is complicated by limitations on spatial and temporal resolution (~20 nm at 20 fps; Figure S2A). Changes in motion more rapid than the frame rate will be missed, and confinement cannot be observed if the object doesn't encounter the barrier during the imaging time. Finally, the cytoplasm is a heterogeneous viscoelastic environment, so care must be taken when interpreting the source of motions. We have tried to address these caveats by controlling our imaging and analysis conditions as detailed below and in the Supplemental Information.

Motion was characterized using mean-squared displacement (MSD) analysis:

$$MSD = \langle r^2 \rangle = 4Dt^{\alpha} + 2\sigma^2, \qquad \text{(Equation 1)}$$

where D is the diffusion coefficient, t is the time lag, α is the scaling exponent, and σ is the measurement error which was fixed at 20 nm (Figures S2A and S2B). The α scaling exponent was used to classify motion as directed ($\alpha > 1.45$), diffusive ($0.4 < \alpha < 1.45$), or confined ($\alpha < 0.4$) (Figure S2B; see the Supplemental Experimental Procedures) [17]. We also used an independent method to characterize the area explored by an endosome, the two-dimensional radius of gyration (Rg^{2D}) (Figure S2C and Equation S1). All motion analysis was performed using a short sliding time window (2.25 s) to capture the heterogeneity within individual trajectories. This time window allowed recovery of α and D to within 15% in simulated trajectories (Table S2).

We characterized the motion parameters α, D, and Rg^{2D} for all EGF-Qdots, ~10 min after their addition to cells, to ensure they were internalized into early endosomes. Analysis of EGF-Qdot trajectories indicated that the majority (59% ± 9%) of the EGF-Qdot lifetime was confined (median α = 0.32 ± 0.09; Table 1). To investigate the motion specifically for the motile population of EGF-Qdots, we selected only the subset of trajectories containing directed movement (net displacement > 1 μm and $\alpha > 1.5$ for 1 s) for analysis (Figure S2D). Even in this set of motile trajectories, only 23% ± 8% of the endosomal lifetime was directed (Table 1). The majority of the time (52% ± 12%) the motion in these motile trajectories was diffusive (median α = 0.84 ± 0.24, Table 1), suggesting that pauses are diffusive and distinct from the confined, immotile population.

The Actin Network Regulates the Confinement of Early Endosomes

To obtain insight into the regulation of different types of endosomal motion, we investigated the effects of one potential modulator, the actin cytoskeleton. Previous studies suggested that actin could play several roles, including forming a restrictive cage [10] that may used by myosins to tether endosomes [9], serving as a track for myosin-driven transport [10], or polymerization of *Listeria*-like actin comet tails to generate propulsive forces [18] (Figure 2A). These roles predict that actin disruption would either increase endosomal motion (caging and tethering) or decrease endosomal motion (myosin transport and propulsion).

We tested these models by measuring changes in motility parameters for all EGF-Qdots in the same cell before and after a 5 min drug perturbation of the actin cytoskeleton. Cells were treated with latrunculin B to depolymerize actin filaments, jasplakinolide to stabilize and increase the density of the actin network, or nocodazole to disrupt directed motion by depolymerizing the majority of MT tracks (Figure S2E). As expected, nocodazole treatment significantly lowered the median α, D, and Rg^{2D} and the amount of directed motion (Figures 2B and 2C). In contrast, treatment of cells with latrunculin B significantly increased the median α, D, and Rg^{2D} (Figure 2B). These endosomes exhibited less confinement and more diffusive motion, but directed motion was unchanged (Figure 2C). Stabilization of actin filaments with jasplakinolide significantly decreased directed movement (Figure 2C). These effects suggest that the dominant role played by actin is restriction of early endosomal motion (caging and tethering).

To address the role of actin in regulating early endosomal motion specifically during directed trafficking, we selectively analyzed motile tracks (Figure 2D). Analysis of this subset of tracks showed no significant effect of latrunculin B or jasplakinolide (Figures 2E and 2F), suggesting that actin density does not affect the motion of early endosomes once directed transport has commenced.

The Transition Periods before and after Directed Runs Are Diffusive

We objectively parsed Rab5-positive, motile EGF-Qdot trajectories into directed runs and pauses to allow analysis of the motion in these two phases separately and to investigate the

Table 1. Motion Characteristics of EGF-Qdots

	α	D ($\mu m^2/s$)	Rg^{2D} (μm, over 0.75 s)	Confined ($\alpha < 0.4$)	Diffusive ($0.4 < \alpha < 1.45$)	Directed ($\alpha > 1.45$)
All trajectories	0.32 ± 0.09	0.006 ± 0.001	0.0016 ± 0.0003	59% ± 9%	39% ± 9%	2% ± 1%
Motile trajectories	0.84 ± 0.24	0.024 ± 0.023	0.0067 ± 0.0055	25% ± 13%	52% ± 12%	23% ± 8%

MSD and Rg^{2D} analysis was performed on EGF-Qdot trajectories from 30 s movies (acquired at 20 fps) in 40 cells using a 2.25 s sliding time window (analysis description in Figures S2B and S2C). The median values of α, D, and Rg^{2D} were calculated for each cell; table values are means ± SEMs for all cells. See also Figure S2 and Table S2.

temporal relationship between changes in motion (Figures 3A, S3A, and S3B). Two criteria were used to determine the position of directed runs: a directional correlation algorithm, termed the speed correlation index (SCI) [20], and the instantaneous speed (Figures 3B, S3C, and S3D and Table S3).

The directed runs exhibited α exponents from MSD fits >1.45 (Figures 3B and 3C), independently supporting our parsing criteria. The lifetime (T_{av} = 1.2 s; Figure S3F) of the directed runs was longer than that of individual dynein runs in vitro [21], suggesting that multiple dynein motors are present. Consistent with previous work [16, 22], early endosomes achieved very high instantaneous speeds (2–4 μm/s; Figure S3G). Since increasing the number of dyneins in vitro does not enhance minus-end-directed speeds [23], additional factors in the cell likely promote faster dynein motility. We found that pauses had a longer average lifetime than directed runs (T_{av} = 4.7 s; Figure S3H) and a broader range of α values, although the majority (65%) were diffusive (Figure 3C). MSD analysis of the longest pauses observed, without use of a sliding time window, yielded similar results (Figures S3I–S3K), indicating that pauses are diffusive over longer time scales.

Isolating the periods immediately before and after a directed run provides insight into the initiation and termination of directed trafficking in the cell since it is during these transition periods when motors are either engaged or halted. The motions immediately before and after directed runs were diffusive (Figures 3A and 3D and Table S4). The diffusion coefficients for

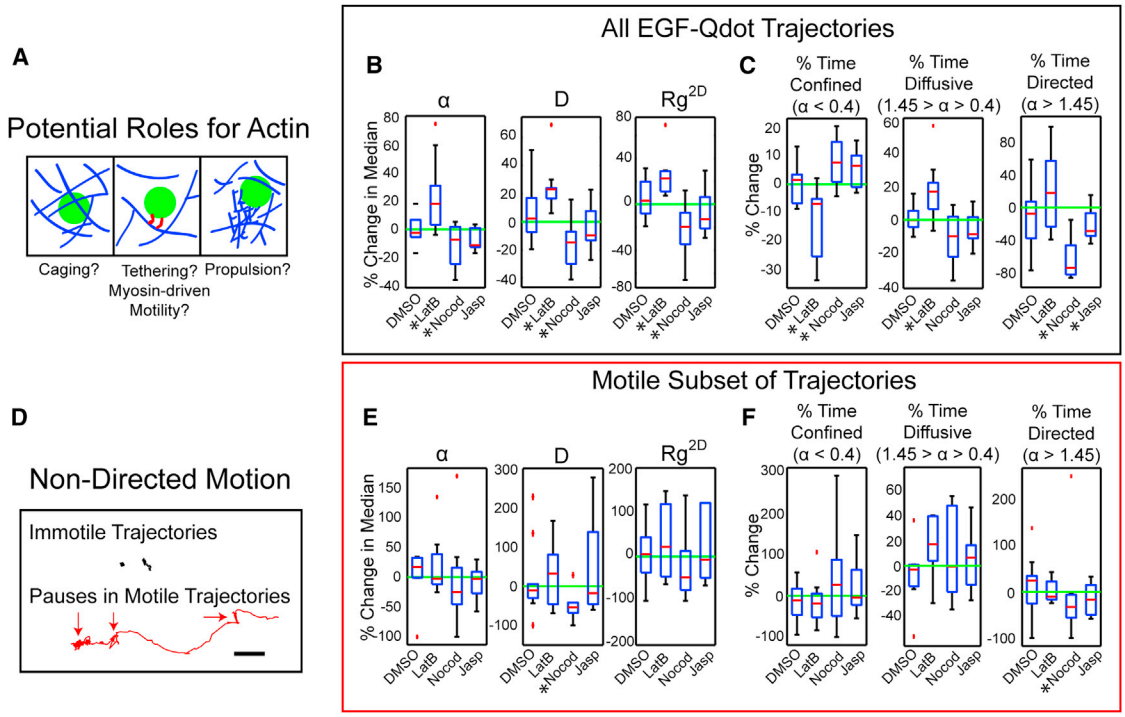

Figure 2. The Effect of Cytoskeletal Disruption on Early Endosomal Motion

(A) Potential roles for actin filaments in early endosomal movement. Early endosomes (green), actin filaments (blue), and myosin motors (red) are shown.

(B) The effect of cytoskeletal perturbations on endosomal motion. All EGF-Qdot trajectories were analyzed for the indicated parameters using a sliding time window of 2.25 s, and the percent change in the median value per cell was calculated (n = 10 cells). DMSO, dimethyl sulfoxide control; LatB, 1 μM latrunculin B; Nocod, 10 μg/ml nocodazole; Jasp, 100 nM jasplakinolide. For all boxplots, medians (red lines), 25th and 75th percentiles (box edges), data extremes (whiskers), outliers (red crosses), and 0% change (green lines) are shown. Significant changes (*p < 0.05) were determined using a binomial test of the percent change in the median. See also Table 1 and Figure S2.

(C) The effect of cytoskeletal perturbations on the percentage of time EGF-Qdots spend confined, diffusive, or directed.

(D) Early endosomal trajectories contain two types of nondirected movement. An immotile set of trajectories lacks directed movement for the entire period of observation. In contrast, motile trajectories contain periods of directed movement but also pauses (arrows). The scale bar represents 2 μm.

(E) The effect of cytoskeletal perturbations on the motion of the motile subset of trajectories.

(F) The effect of cytoskeletal perturbations on the percentage of time EGF-Qdots spend confined, diffusive, or directed in the motile subset.

See also Figure S2 and Table S2.

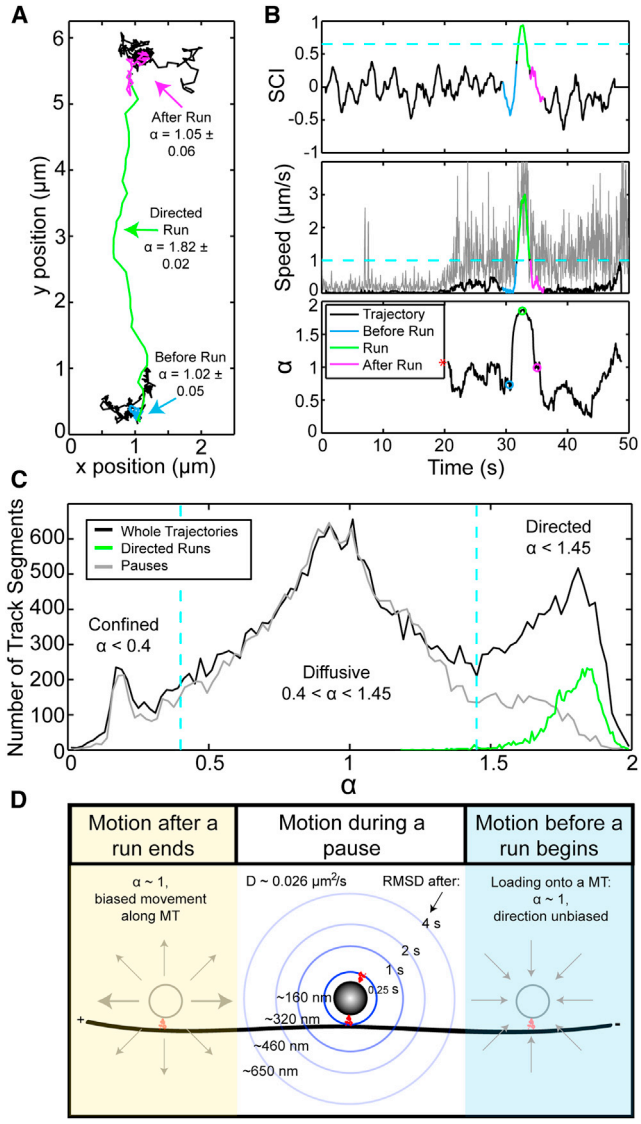

Figure 3. Parsing of Trajectories into Directed Runs and Pauses

(A) Early endosomal trajectories exhibited directed motion punctuated by pauses. A representative EGF-Qdot trajectory (black) with directed motion (green) and 2.25 s immediately before (blue) and after (magenta) the run highlighted. For α values (means ± SEMs), n = 71 before run, n = 29 directed run, and n = 54 after run. See also Figure S3.

(B) Track parsing criteria and motion analysis. The directed movement criteria (SCI and instantaneous speed [position smoothed over 1.2 s; unfiltered data in gray]) and the MSD α scaling exponent using a 2.25 s sliding window (Figure S2B and Table S2) are shown for the trajectory in (A) (5% false-positive thresholds in cyan [Figures S3C–S3E and Table S3]). Circles highlight the α values immediately before and after the run and the run center. The α values before the red asterisk were unreliable due to poor MSD fitting and are not plotted.

(C) MSD motion analysis of intact trajectories, directed runs, and pauses using a 2.25 s sliding time window. Whole tracks, 7% confined, 65% diffusive, and 28% directed; directed runs, 0% confined, 1% diffusive, and 99% directed; and pauses, 7% confined, 82% diffusive, and 11% directed.

(D) Characteristics of early endosomal motion after a run, during a pause, and before a run begins. An approximately scaled drawing of an early endosome (~200 nm diameter), its linkage to the MT track via dynein (~70 nm, adapted from [19]), and its predicted diffusion (root mean squared displacement (RMSD), blue circles) after different time intervals are shown.

See also Figures S2 and S3 and Tables S2–S4.

Table 2. Spatial Correlation between Rab5-Positive Endosomal Pauses and Organelle Positions

	Spatial Overlap with Rab5 Pauses	Spatial Overlap with Random Locations	Number of Pauses Scored
Rab5*	25% ± 12%	11% ± 4%	89
Late endosomes/ lysosomes	21% ± 9%	25% ± 6%	110
Mitochondria	5% ± 4%	12% ± 8%	90
Golgi	4% ± 4%	6% ± 7%	90
ER*	39% ± 13%	23% ± 8%	76

The cellular location of pauses in GFP-Rab5-positive early endosomal directed runs was determined and scored for the presence of the indicated organelle (see the Supplemental Experimental Procedures for organelle constructs). Mean percent ± SEM is shown; n = 5 cells, with ten Rab5 tracks per cell. Statistical significance (*p < 0.05) was determined by comparison of the percent of endosomal pauses that correlated with the location of each organelle to the percent of randomly chosen locations that correlated with that organelle.

these periods were similar to each other (before D = 0.024 ± 0.030 $\mu m^2/s$, after D = 0.028 ± 0.018 $\mu m^2/s$), to D values for entire pauses (Figure S3K), and to measurements of D for other organelles [24]. The motion occurring after a directed run, although diffusive, had a significant (~2-fold) enrichment of motion aligned with the MT axis (Figures S3L and 3D). This suggests that after the end of a directed run endosomes maintain a transient connection to the MT.

Interactions with Organelles Spatially Correlate with Early Endosome Pause Locations

We investigated factors that may trigger pauses in directed transport by spatially correlating the sites of pausing with two aspects of cellular architecture likely to affect cargo trafficking: (1) the presence of other organelles and (2) the local organization of the MT network.

To determine whether interactions between early endosomes and organelles contribute to pauses, we compared the location of GFP-Rab5-positive endosomal pauses with the position of other organelles. The Golgi, mitochondria, and late endosomes/lysosomes showed no significant spatial correlation (Table 2). In contrast, a significant percentage of pauses spatially correlated with the location of both other Rab5-positive endosomes (25% ± 2%; $p < 0.05$) and ER tubules (39% ± 13%; $p < 0.05$, Table 2), relative to randomly chosen locations. We further investigated these two organelle interactions in the following sections.

Early Endosomal Membrane Tension May Regulate the Pauses in Directed Motion

Sparse labeling of early endosomes with EGF-Qdots allowed us to track individual early endosomes relative to the dense total GFP-Rab5 population. EGF-Qdots underwent multiple rounds of merging and splitting from other GFP-Rab5 punctae during trafficking (Figure 4A and Movie S2). The motions during pauses when two early endosomes merged were diffusive (Figure 4B), suggesting that either the two endosomes moved diffusively together or that the confinement induced by their interaction was brief.

Some interruptions in minus-end-directed transport were associated with rapid reversals in direction (Figure 4Ci and Movie S3, left) at speeds exceeding that of molecular motors (>30 μm/s; Figure 4Cii). Even after this very abrupt change in motion, the pauses were diffusive

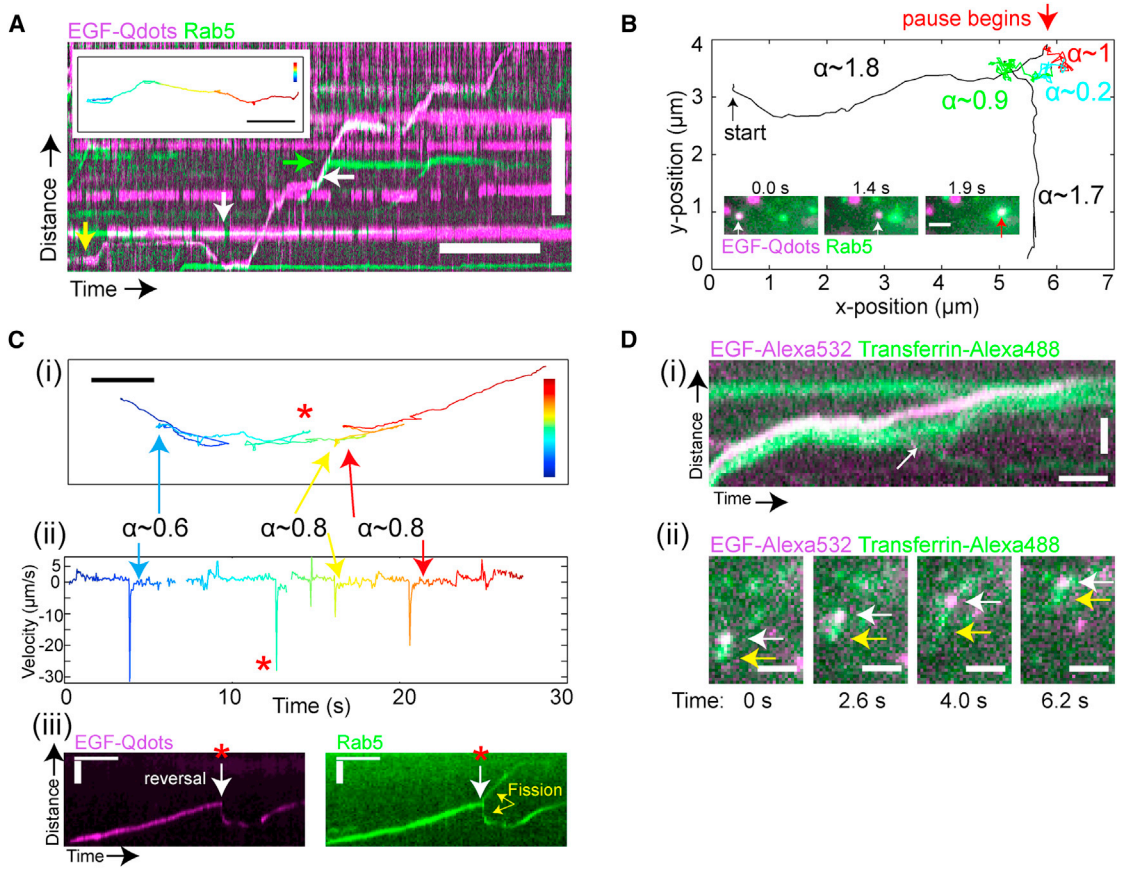

Figure 4. The Motion of Individual EGF-Qdot-Containing Early Endosomes during Encounters with Other Rab5-Positive Early Endosomes

(A) EGF-Qdots merge with and split away from other early endosomes during their trafficking. A kymograph showing an EGF-Qdot (magenta, yellow arrow) relative to several other GFP-Rab5 punctae (green) that merge (white arrows) and split away (green arrow) is presented. Scale bars represent 5 μm and 5 s. The inset shows an x,y trajectory color coded for time (blue, first frame; red, last frame). The scale bar represents 5 μm. See also Movie S2.

(B) Pauses in early endosomal motility that occur during an encounter with another early endosome are mainly diffusive. The trajectory (black) of an EGF-Qdot that interacts with another endosome during a pause (three time regions with distinct α are color coded on the plot during the pause: red, cyan, and green). The inset images show the EGF-Qdot-containing endosome (magenta, white arrow) moving toward a large GFP-Rab5-positive endosome and pausing (red arrows). The scale bar represents 2 μm.

(C) An extreme example of a GFP-Rab5/EGF-Qdot particle snapping backward after several periods of directed motion. The trajectory is color coded for time (blue, first frame; red, last frame) is shown in (Ci). The scale bar represents 5 μm. (Cii) shows the instantaneous velocity of the trajectory in (Ci). The α values for three pause locations are indicated with arrows. The kymographs in (Ciii) show one of the EGF-Qdot reversals (white arrow, red asterisk marks time-point of the reversals in Ci and Cii) during which a puncta of GFP-Rab5 separates from the EGF-Qdot/GFP-Rab5 (yellow arrows) as the EGF-Qdot snaps backward. Scale bars represent 2 μm and 2 s. See also Movie S3.

(D) Transferrin-positive tubules extend from motile, EGF-positive endosomes. A kymograph showing a pause in EGF-Alexa532/transferrin-Alexa488 trafficking and a fission event (white arrow) is presented in (Di). Scale bars represent 2 μm and 1 s. (Dii) shows a montage from the movie in (Di) of EGF (magenta, white arrow) and transferrin (green, yellow arrow).

Movies S2 and S3.

(α ~0.6–0.8; Figures 4Ci and 4Cii). These rapid reversals suggest that some pauses in directed motion correlate with tension on the endosomal membrane, an elastic structure that can recoil rapidly. Figure 4Ciii highlights one reversal in which fission appears to occur when the GFP-Rab5 signal splits into two dimmer particles (Movie S3, right). During sorting of endosomal cargo, transferrin-positive tubules extend from EGF punctae and eventually undergo fission to enter the recycling pathway [25]. We observed transferrin-positive tubules extending toward the cell periphery and undergoing fission as the attached EGF punctae moved rapidly (~2 μm/s) toward the perinuclear region (Figure 4D). This suggests that the directed movement of early endosomes must be coordinated with membrane tension in the larger tubular network, which sometimes results in fission and membrane recoil events.

Early Endosomes Deform the ER during Trafficking

To investigate the effect of interactions between early endosomes and the ER, we looked for correlated movement of these two organelles before or during pauses. We observed long-lived interactions that resulted in dramatic and rapid ER deformation in both Arpe-19 and COS-7 cells (Figures 5A–5C and S4A and Movie S4, left). We also saw instances of Rab5 punctae at the front of newly extending ER tubules (Figures 5B and 5C and Movie S4, right). The long lifetimes of these attachments and the requirement for endosome-generated force to deform the ER for continued directed movement

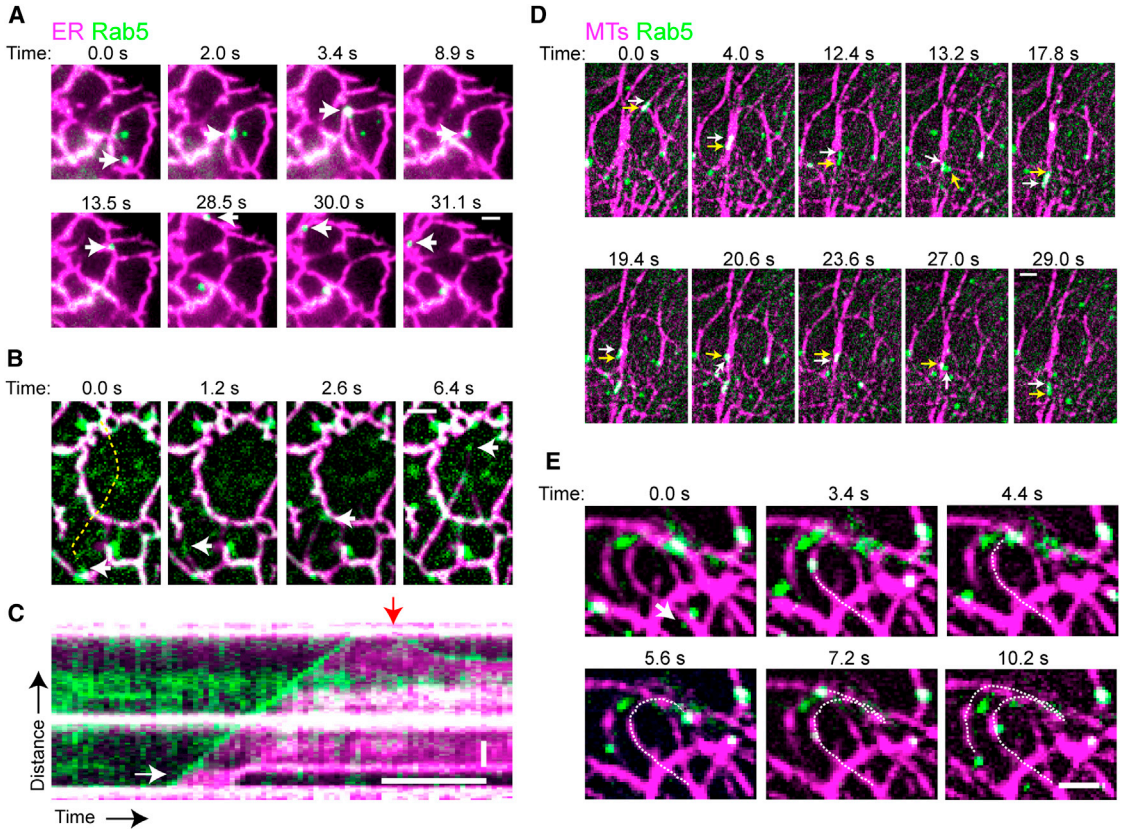

Figure 5. Early Endosomal Movement Is Affected by Interactions with the ER and Multiple MTs

(A) Early endosomes remain attached to the ER for long periods during which repeated deformation of the ER occurs. The white arrow follows the same early endosome. The scale bar represents 2 μm. See also Movie S4, left.

(B) An early endosome appears to pull an ER tubule behind it during a directed run. The yellow dotted line in the first panel indicates the trajectory used to generate the kymograph in (C). Images are background subtracted. The scale bar represents 2 μm. See also Movie S4, right.

(C) The kymograph highlights the rapid (~1.6 μm/s) movement of the early endosome (green, white arrow) toward the perinuclear region followed by a slower reversal (~0.7 μm/s, red arrow). Scale bars represent 4 s and 2 μm. See also Movie S4, right, and Figure S4A.

(D) Pausing and rotation of two elongated early endosomes at a region of dense MTs. The white and yellow arrows indicate the two ends of an elongated early endosome (green) to highlight its rotation during the pause near dense MTs (magenta). The two rows show different early endosomes navigating the same region. Images are background subtracted. The scale bar represents 2 μm. See also Movie S5, left.

(E) Rapid switch between 2 MT tracks by an early endosome. The dotted white line indicates the trajectory taken by the early endosome (green, arrow). Images are background-subtracted. The scale bar represents 2 μm. See also Movie S5, right, and Figure S4B.

See also Figure S4 and Movies S4 and S5.

suggest that this type of membrane contact site is a previously unappreciated regulator of early endosomal motility.

Early Endosomal Motion Is Influenced by MT Organization

To investigate how MT track organization affects early endosomal movement, we imaged GFP-Rab5 simultaneously with 2xmCherry-EMTB, the microtubule binding domain of the microtubule associated protein (MAP) ensconsin [26]. Pausing of GFP-Rab5-positive endosome runs occurred at regions of dense, apparently intersecting MTs (ten out of ten cells; Figure 4D and Movie S5, left). In eight out of ten cells, we observed a few elongated early endosomes that were large enough to enable visualization of rotations, deformations, and sometimes fissions during pauses in MT dense regions (eight out of eight cells; Figure 5D and Movie S5, left). However, we also observed sharp changes in direction without measurable pausing, which we interpret as MT track switching (ten out of ten cells; Figure 5E and Movie S5, right). Although the high MT density in Arpe-19 cells prevented us from quantifying the contribution of MT intersections to pausing, frequent MT track switching and pauses at MT-enriched regions were also observed in parallel studies in COS-7 cells (Figure S4B). These observations suggest that MT track organization impacts early endosomal movement, potentially through multiple motors on the endosome engaging different MTs.

Discussion

Early Endosomes Contain Subpopulations with Distinct Motility Characteristics, Differentially Regulated by the Actin Cytoskeleton

Our high-resolution imaging of early endosomal dynamics and motion classification suggests there are two subpopulations of early endosomes that differ in both their motility characteristics and regulation by the actin cytoskeleton. Immotile (moving < 0.5 μm over 45 s) endosomes were confined by the actin network (Table 1 and Figured 2B and 2C). Motile early endosomes contained directed runs and diffusive pauses unaffected by perturbation of the actin cytoskeleton (Table 1, Figure 2E, 2F, 3, and S3I–S3K, and Table S4). Stabilization of

the actin network decreased the amount of directed movement in the whole population (Figure 2C), supporting a model in which confinement of peripheral early endosomes by actin regulates the initiation of directed transport. Myosin VI is required for endosomes to navigate the actin-rich cell periphery in some cell types [10]. The reduced localization of myosin VI-GFP to motile early endosomes (Figure S1C) and the decreased density of the actin filaments in the cell interior near MTs (Figure S1A) suggests that both changes in endosomal actin-interacting proteins and local changes in the actin cytoskeleton may contribute to the lack of an effect of actin disruption on motile early endosomes.

The directed runs are MT and dynein/dynactin dependent [16] (Movie S1), and the majority are directed toward MT minus ends in the perinuclear region. Some pauses in directed transport appear to be initiated by a tug-of-war between motors engaging different MTs (Figure 5D), suggesting that dynein may be engaging in a tug-of-war with itself. However, early endosomes also associate with MT plus-end-directed kinesins despite their lack of bidirectional movement (Figure S1D) [12, 13, 15]. One possibility is that a low ratio of kinesins to dyneins creates a tug-of-war that manifests as a pause, but dynein ultimately wins.

The Motion during Pauses Is Diffusive

The diffusive nature (α scaling exponent of MSD plots $\sim$1) of endosomal motion during pauses in directed transport (Table 1, Figures 3 and S3I–S3K, and Table S4) indicates that the endosomal motion is randomly directed, but does not restrict that motion to free diffusion. Types of movement suggested to result in diffusive scaling in two dimensions include free diffusion in the cytoplasm [27], the movement of motors on mixed polarity filaments [28], or tethering through a long and/or flexible linkage [29]. Diffusive scaling in one dimension can result from a tug-of-war between mixed polarity motors [30] or diffusion of a MAP or motor along the MT lattice [21]. Movement of myosins along mixed polarity actin filaments is unlikely since actin perturbations did not affect endosomal motion during pauses (Figures 2E and 2F), and movement along mixed polarity MTs is also unlikely because the MTs are radially arrayed (Figure S1A). Since the periods immediately after a directed run had alignment with the MT track (Figure S3L), interactions requiring continued interactions between the early endosome and MT, such as a bidirectional tug-of-war between MT motors or diffusion of a MAP or motor, could occur. However, since the distance that a diffusing endosome (D $\sim$0. 026 $\mu m^2/s$) is expected to move during the average pause lifetime (T_{av} = 4.7 s) is $\sim$700 nm, about 10-fold greater than dynein's length [19], and the movement was randomly directed before a directed run commenced (Figure S3L), the endosome likely detaches from the MT at some point during pauses (Figure 3D).

High Endosomal Membrane Tension May Induce Pausing and Facilitate Cargo Sorting

The location of endosomal pauses overlapped with MT intersections (Figures 5D and S4B and Movie S5, left), other early endosomes (Table 2, Figure 4B, and Movie S2), and ER tubules (Table 2, Figures 5A–5C and S4A, and Movie S4). We hypothesize that, rather than acting as random obstacles to directed movement, interactions with these structures, and the consequent pauses, contribute functionally to cargo sorting.

Rab5 forms microdomains on larger tubular endosomal structures involved in cargo sorting [31]. Instead of a motor-motor tug-of-war, a tug-of-war may occur between the dynein-driven movement of Rab5 microdomains and the tension in the attached tubular-vesicular endosome. The extremely rapid reversals in direction (>30 μm/s; Figure 4Cii and Movie S3) and deformation and fission of early endosomes (Figure 4Ciii; Movie S3, right; Figure 5D; and Movie S5, left) indicate membrane tension is high during pauses.

In vitro studies have demonstrated that teams of kinesin-1s can tubulate a model vesicle [32]. However, the stall force of dynein ($\sim$1 pN) is lower than that of kinesin-1 ($\sim$6 pN) [2], and studies estimating the number of motors on other endosomal populations suggested that only a few motors are present [34]. A small team of dynein motors could thus be stalled by tension in the membranes during sorting. Since dynein is a flexible motor, capable of backstepping to avoid obstacles [21, 35] and acting as a gear under load [33], it may be well adapted to handle this backward pulling force and maintain contact with the MT for continued tubule extension and efficient sorting.

Early endosomal connections result in dramatic deformation and tubulation of the ER (Figures 5A–5C and S4A and Movie S4). Contacts between early endosomes and the ER facilitate dephosphorylation of active receptor tyrosine kinases like EGFR by the ER resident phosphatase PTP1B [36]. At the ultrastructural level, the ER and endosomal membranes are closely approximated (<30 nm) and bridged by unidentified protein fibrils [37]. The force required to maintain an extended tubule from the ER in vitro is $\sim$20 pN, even in the presence of cytosol [38]. Since many organelles contact the ER [6], understanding how the force required to deform the ER affects motility is relevant to many trafficking pathways. Conversely, the ability of motile organelles to deform and tubulate the ER may contribute to the maintenance of ER structure and distribution.

Conclusions

Our high-resolution tracking and motion analysis demonstrated that there is a population of immotile, confined early endosomes that are regulated by actin network density and motile early endosomes undergoing a combination of directed, dynein-driven movement and diffusive pauses. Early endosomal interactions with MT intersections, other early endosomes, and the ER likely contribute to pausing in directed movements. These interruptions in dynein-driven transport may play functional roles such as facilitating early endosomal cargo sorting and maintenance of ER structure.

Experimental Procedures

Detailed materials and methods are available in the Supplemental Experimental Procedures.

Supplemental Information

Supplemental Information includes Supplemental Experimental Procedures, four figures, four tables, and five movies and can be found with this article online at http://dx.doi.org/10.1016/j.cub.2013.05.015.

Acknowledgments

We would like to thank the investigators listed in Supplemental Experimental Procedures for generous sharing of plasmids and software, Martin Pring for consultation on statistics, and Jennine Dawicki McKenna, Roger E. Goldman, and Adam G. Hendricks for assistance with microscopy and programming. NIH funding was from grant numbers P01GM087253 (to E.L.F.H., E.M.O., and Y.E.G.) and T32 GM-07229 (to A.L.Z.).

Received: January 17, 2013
Revised: April 11, 2013
Accepted: May 9, 2013
Published: June 13, 2013

References

1. Lippincott-Schwartz, J., Roberts, T.H., and Hirschberg, K. (2000). Secretory protein trafficking and organelle dynamics in living cells. Annu. Rev. Cell Dev. Biol. *16*, 557–589.
2. Mallik, R., and Gross, S.P. (2004). Molecular motors: strategies to get along. Curr. Biol. *14*, R971–R982.
3. Semenova, I., Burakov, A., Berardone, N., Zaliapin, I., Slepchenko, B., Svitkina, T., Kashina, A., and Rodionov, V. (2008). Actin dynamics is essential for myosin-based transport of membrane organelles. Curr. Biol. *18*, 1581–1586.
4. Schuh, M. (2011). An actin-dependent mechanism for long-range vesicle transport. Nat. Cell Biol. *13*, 1431–1436.
5. Parton, R.M., Hamilton, R.S., Ball, G., Yang, L., Cullen, C.F., Lu, W., Ohkura, H., and Davis, I. (2011). A PAR-1-dependent orientation gradient of dynamic microtubules directs posterior cargo transport in the Drosophila oocyte. J. Cell Biol. *194*, 121–135.
6. Elbaz, Y., and Schuldiner, M. (2011). Staying in touch: the molecular era of organelle contact sites. Trends Biochem. Sci. *36*, 616–623.
7. Zhou, H.X., Rivas, G., and Minton, A.P. (2008). Macromolecular crowding and confinement: biochemical, biophysical, and potential physiological consequences. Annu Rev Biophys *37*, 375–397.
8. Sorkin, A., and Goh, L.K. (2009). Endocytosis and intracellular trafficking of ErbBs. Exp. Cell Res. *315*, 683–696.
9. Provance, D.W., Jr., Addison, E.J., Wood, P.R., Chen, D.Z., Silan, C.M., and Mercer, J.A. (2008). Myosin-Vb functions as a dynamic tether for peripheral endocytic compartments during transferrin trafficking. BMC Cell Biol. *9*, 44.
10. Aschenbrenner, L., Lee, T., and Hasson, T. (2003). Myo6 facilitates the translocation of endocytic vesicles from cell peripheries. Mol. Biol. Cell *14*, 2728–2743.
11. Raposo, G., Cordonnier, M.N., Tenza, D., Menichi, B., Dürrbach, A., Louvard, D., and Coudrier, E. (1999). Association of myosin I alpha with endosomes and lysosomes in mammalian cells. Mol. Biol. Cell *10*, 1477–1494.
12. Loubéry, S., Wilhelm, C., Hurbain, I., Neveu, S., Louvard, D., and Coudrier, E. (2008). Different microtubule motors move early and late endocytic compartments. Traffic *9*, 492–509.
13. Hoepfner, S., Severin, F., Cabezas, A., Habermann, B., Runge, A., Gillooly, D., Stenmark, H., and Zerial, M. (2005). Modulation of receptor recycling and degradation by the endosomal kinesin KIF16B. Cell *121*, 437–450.
14. Aniento, F., Emans, N., Griffiths, G., and Gruenberg, J. (1993). Cytoplasmic dynein-dependent vesicular transport from early to late endosomes. J. Cell Biol. *123*, 1373–1387.
15. Driskell, O.J., Mironov, A., Allan, V.J., and Woodman, P.G. (2007). Dynein is required for receptor sorting and the morphogenesis of early endosomes. Nat. Cell Biol. *9*, 113–120.
16. Flores-Rodriguez, N., Rogers, S.S., Kenwright, D.A., Waigh, T.A., Woodman, P.G., and Allan, V.J. (2011). Roles of dynein and dynactin in early endosome dynamics revealed using automated tracking and global analysis. PLoS ONE *6*, e24479.
17. Berg, H.C. (1993). Random Walks in Biology, Expanded Edition (Princeton: Princeton University Press).
18. Taunton, J., Rowning, B.A., Coughlin, M.L., Wu, M., Moon, R.T., Mitchison, T.J., and Larabell, C.A. (2000). Actin-dependent propulsion of endosomes and lysosomes by recruitment of N-WASP. J. Cell Biol. *148*, 519–530.
19. Vale, R.D. (2003). The molecular motor toolbox for intracellular transport. Cell *112*, 467–480.
20. Bouzigues, C., and Dahan, M. (2007). Transient directed motions of GABA(A) receptors in growth cones detected by a speed correlation index. Biophys. J. *92*, 654–660.
21. Ross, J.L., Wallace, K., Shuman, H., Goldman, Y.E., and Holzbaur, E.L. (2006). Processive bidirectional motion of dynein-dynactin complexes in vitro. Nat. Cell Biol. *8*, 562–570.
22. Lakadamyali, M., Rust, M.J., and Zhuang, X. (2006). Ligands for clathrin-mediated endocytosis are differentially sorted into distinct populations of early endosomes. Cell *124*, 997–1009.
23. Mallik, R., Petrov, D., Lex, S.A., King, S.J., and Gross, S.P. (2005). Building complexity: an in vitro study of cytoplasmic dynein with in vivo implications. Curr. Biol. *15*, 2075–2085.
24. Luby-Phelps, K. (2000). Cytoarchitecture and physical properties of cytoplasm: volume, viscosity, diffusion, intracellular surface area. Int. Rev. Cytol. *192*, 189–221.
25. Mesaki, K., Tanabe, K., Obayashi, M., Oe, N., and Takei, K. (2011). Fission of tubular endosomes triggers endosomal acidification and movement. PLoS ONE *6*, e19764.
26. Faire, K., Waterman-Storer, C.M., Gruber, D., Masson, D., Salmon, E.D., and Bulinski, J.C. (1999). E-MAP-115 (ensconsin) associates dynamically with microtubules in vivo and is not a physiological modulator of microtubule dynamics. J. Cell Sci. *112*, 4243–4255.
27. Wirtz, D. (2009). Particle-tracking microrheology of living cells: principles and applications. Annu Rev Biophys *38*, 301–326.
28. Nelson, S.R., Ali, M.Y., Trybus, K.M., and Warshaw, D.M. (2009). Random walk of processive, quantum dot-labeled myosin Va molecules within the actin cortex of COS-7 cells. Biophys. J. *97*, 509–518.
29. Gu, Y., Sun, W., Wang, G., Jeftinija, K., Jeftinija, S., and Fang, N. (2012). Rotational dynamics of cargos at pauses during axonal transport. Nat Commun *3*, 1030.
30. Müller, M.J., Klumpp, S., and Lipowsky, R. (2010). Bidirectional transport by molecular motors: enhanced processivity and response to external forces. Biophys. J. *98*, 2610–2618.
31. Sönnichsen, B., De Renzis, S., Nielsen, E., Rietdorf, J., and Zerial, M. (2000). Distinct membrane domains on endosomes in the recycling pathway visualized by multicolor imaging of Rab4, Rab5, and Rab11. J. Cell Biol. *149*, 901–914.
32. Koster, G., VanDuijn, M., Hofs, B., and Dogterom, M. (2003). Membrane tube formation from giant vesicles by dynamic association of motor proteins. Proc. Natl. Acad. Sci. USA *100*, 15583–15588.
33. Mallik, R., Carter, B.C., Lex, S.A., King, S.J., and Gross, S.P. (2004). Cytoplasmic dynein functions as a gear in response to load. Nature *427*, 649–652.
34. Hendricks, A.G., Perlson, E., Ross, J.L., Schroeder, H.W., 3rd, Tokito, M., and Holzbaur, E.L. (2010). Motor coordination via a tug-of-war mechanism drives bidirectional vesicle transport. Curr. Biol. *20*, 697–702.
35. Dixit, R., Ross, J.L., Goldman, Y.E., and Holzbaur, E.L. (2008). Differential regulation of dynein and kinesin motor proteins by tau. Science *319*, 1086–1089.
36. Haj, F.G., Verveer, P.J., Squire, A., Neel, B.G., and Bastiaens, P.I. (2002). Imaging sites of receptor dephosphorylation by PTP1B on the surface of the endoplasmic reticulum. Science *295*, 1708–1711.
37. Eden, E.R., White, I.J., Tsapara, A., and Futter, C.E. (2010). Membrane contacts between endosomes and ER provide sites for PTP1B-epidermal growth factor receptor interaction. Nat. Cell Biol. *12*, 267–272.
38. Upadhyaya, A., and Sheetz, M.P. (2004). Tension in tubulovesicular networks of Golgi and endoplasmic reticulum membranes. Biophys. J. *86*, 2923–2928.